

Electron-Deficient Mo Sites Enhance Electrochemical Nitrate Reduction to Ammonia by Promoting Water Dissociation

Xue Zhou^[a], Wence Xu^[a,b], Yunduo Huang^[a], Zhonghui Gao^[a,b], Yanqin Liang^[a,b], Hui Jiang^[a,b],
Zhaoyang Li^[a,b], Fang Wang^[c]*, Shengli Zhu^[a,b]* and Zhenduo Cui^[a,b]*

[a] School of Materials Science and Engineering, Tianjin University, Tianjin 300350, China

[b] State Key Laboratory of Precious Metal Functional Materials, Tianjin 300350, China

[c] School of Mechanical Engineering, Dongguan University of Technology, Dongguan, 523808, China

Corresponding Author

*Wence Xu. E-mail: wcxu@tju.edu.cn;

* Fang Wang. E-mail: wangfang917@126.com;

* Shengli Zhu. E-mail: slzhu@tju.edu.cn;

Calculation of ammonia yield rate, Faradic efficiency and Energy efficiency.

The ammonia (NH₃) yield rate was calculated using equation (1):

$$\text{Yield}_{\text{NH}_3} = (C_{\text{NH}_3} \times V) / (t \times S) \quad (1)$$

The Faradaic efficiency (FE) was calculated as the ratio of the electrical charge used for NH₃ production to the total electrical charge involved in the overall NITRR process, as shown in equation (2):

$$\text{FE}_{\text{NH}_3} = (8 \times F \times C_{\text{NH}_3} \times V) / Q \quad (2)$$

where C_{NH₃} denotes the concentration of the produced NH₃ (not NH₄⁺-N), V is the volume of the catholyte (40 mL), t is the duration of the potentiostatic test (1 hour), S is the geometric area of the working electrode (0.15 cm²), F is the Faradaic constant (96485 C mol⁻¹), and Q represents the total electrical charge consumed during the entire NITRR process.

The Energy efficiency (EE) was defined as the ratio of fuel energy to applied electrical power, as shown in equation (3):

$$\text{EE}_{\text{NH}_3} = (E^0_{\text{OER}} - E^0_{\text{NH}_3}) \times \text{FE}_{\text{NH}_3} / (E_{\text{OER}} - E_{\text{NH}_3}) \quad (3)$$

Where E⁰_{NH₃} represents the equilibrium potential for the nitrate (NO₃⁻) electroreduction to NH₃ (NITRR), which is 0.69 V versus RHE. E⁰_{NH₃} is the equilibrium potential for oxygen evolution reaction (OER) set at 1.23 V versus RHE. FE_{NH₃} denotes the Faradaic efficiency for NH₃ production. E_{OER} is the applied potential at the anode, which is 1.23 V assuming zero overpotential for OER. E_{NH₃} is the applied potential at the cathode.

Isotope Labeling Experiments

To trace the origin of NH₃, isotope labeling experiments were conducted using 1H-NMR (JEOL JNM-ECZ600R). NO₃⁻ solutions containing ¹⁵NO₃⁻-¹⁵N and ¹⁴NO₃⁻-¹⁴N were used as nitrogen sources for the NO₃⁻ reduction reactions respectively. Following the electrochemical reaction, 0.5 mL of the electrolyte was collected and mixed with 0.1 mL of 4 M H₂SO₄ and 0.25 mg of maleic acid. Finally, 0.05 mL of D₂O was added to the mixture for NMR analysis.

Electron paramagnetic resonance (EPR) spectroscopy for hydrogen radical determination

Hydrogen radicals were detected using EPR spectroscopy with 5,5-dimethyl-1-pyrroline N-oxide (DMPO) as the spin-trapping agent. The electrolyte was first purged with argon for 30 minutes to remove dissolved oxygen, and then DMPO was added to the electrolyte. After 5 minutes of electrolysis at -0.2 V vs. RHE, the electrolyte was analyzed using a Bruker EMX Plus spectrometer.

In-situ electrochemical differential electrochemical mass spectrometry (DEMS) measurements

During the in-situ DEMS measurements, an electrolyte solution consisting of 1 M KOH and 0.1 M NaNO₃ was continuously circulated through the electrochemical cell using a peristaltic pump. LSV was performed from -0.624 to -1.524 V vs. Ag/AgCl at a scan rate of 5 mV s⁻¹. Differential mass signals were recorded when gaseous intermediate products formed on the catalyst surface. Upon completion of each electrochemical test, the corresponding mass signals returned to the baseline. The subsequent cycle was then initiated under same conditions. To avoid accidental error, seven consecutive LSV test cycles were conducted.

Recovery of NH₄Cl solid

After the NITRR test, the electrolyte was heated to 70 °C, and argon (Ar) gas was used to purge the NH₃ gas. The outlet gas stream was directed into a 1 M HCl solution, where NH₄Cl solution was formed. The NH₄Cl powder was subsequently recovered by evaporating the collected solution at 70 °C.

DFT calculations

We used the DFT as implemented in the Vienna Ab initio simulation package (VASP) in all calculations¹. The exchange-correlation potential is described by using the generalized gradient approximation of Perdew-Burke-Ernzerhof (GGA-PBE)². The projector augmented-wave (PAW) method is employed to treat interactions between ion cores and valence electrons³. The plane-wave cutoff energy was fixed to 450 eV. Given structural models were relaxed until the Hellmann-Feynman forces smaller than -0.02 eV/Å and the change in energy smaller than 10⁻⁵ eV was attained. The long-range van der Waals interaction is described by the DFT-D3 approach.

The adsorption energy (E_{ads}) of species is calculated by:

$$E_{\text{ads}} = E(\text{system}) - E(\text{catalyst}) - E(\text{species})$$

where $E(\text{system})$, $E(\text{catalyst})$, and $E(\text{species})$ are the total energy of the optimized system with adsorbed species, the isolated catalyst, and species, respectively.

The Gibbs free energy change is defined as:

$$\Delta G = \Delta E + \Delta \text{ZPE} - T\Delta S$$

where ΔE is the electronic energy calculated with VASP, ΔZPE and ΔS are the zero-point energy difference and the entropy change between the products and reactants, respectively, and T is the temperature (298.15 K).

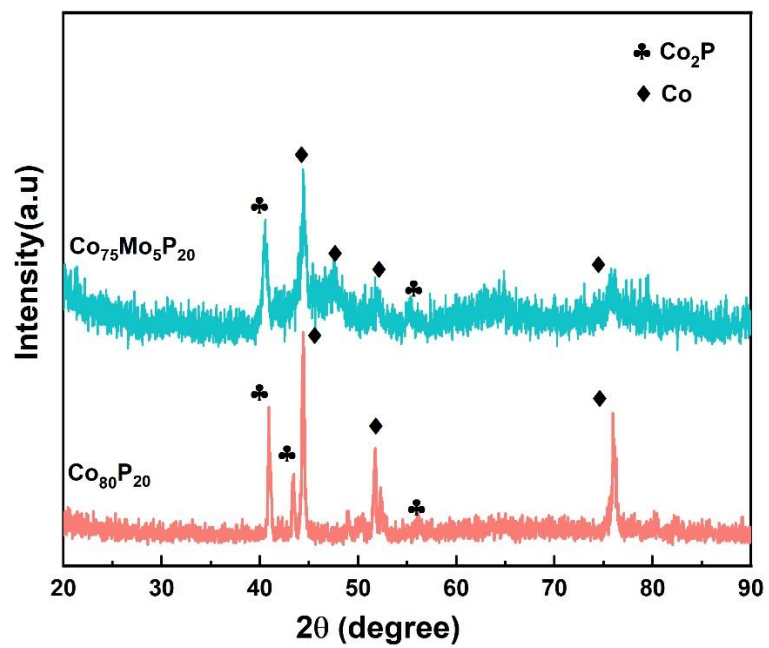


Figure S1. XRD patterns of $\text{Co}_{80}\text{P}_{20}$ and $\text{Co}_{75}\text{Mo}_5\text{P}_{20}$ precursor.

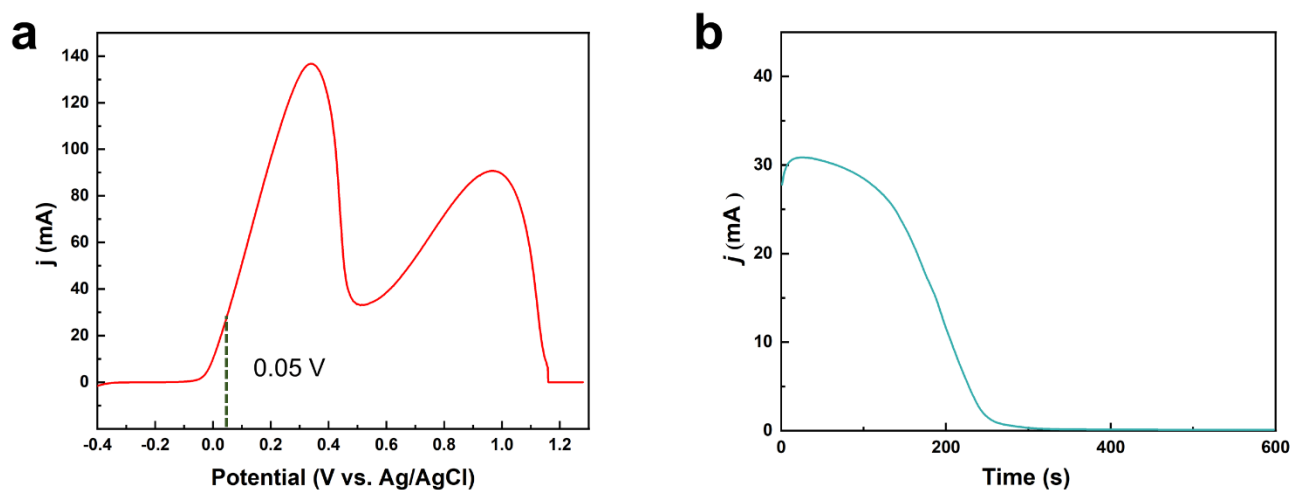


Figure S2. (a) The linear sweep voltammetry curve of the $\text{Co}_{75}\text{Mo}_5\text{P}_{20}$ precursor in 1 M HCl. (b) The $i-t$ curve of dealloying process under -0.5 V vs. Ag/AgCl.

*Two distinct peaks are observed, corresponding to the oxidation (or dissolution) of the Co and Co_2P phases, respectively. The critical dissolution potential for the Co phase is approximately -0.2 V vs. Ag/AgCl, while that for the Co_2P phase is around 0.5 V. By leveraging the significant difference in electrochemical stability between these two phases, the Co phase can be selectively removed via microscopic galvanic corrosion. A dealloying potential of 0.05 V was chosen to selectively dissolve the Co phase while preserving the Mo-doped Co_2P phase. the $i-t$ curve at 0.05 V exhibits a near-zero current, indicating that the Co phase has been completely removed.

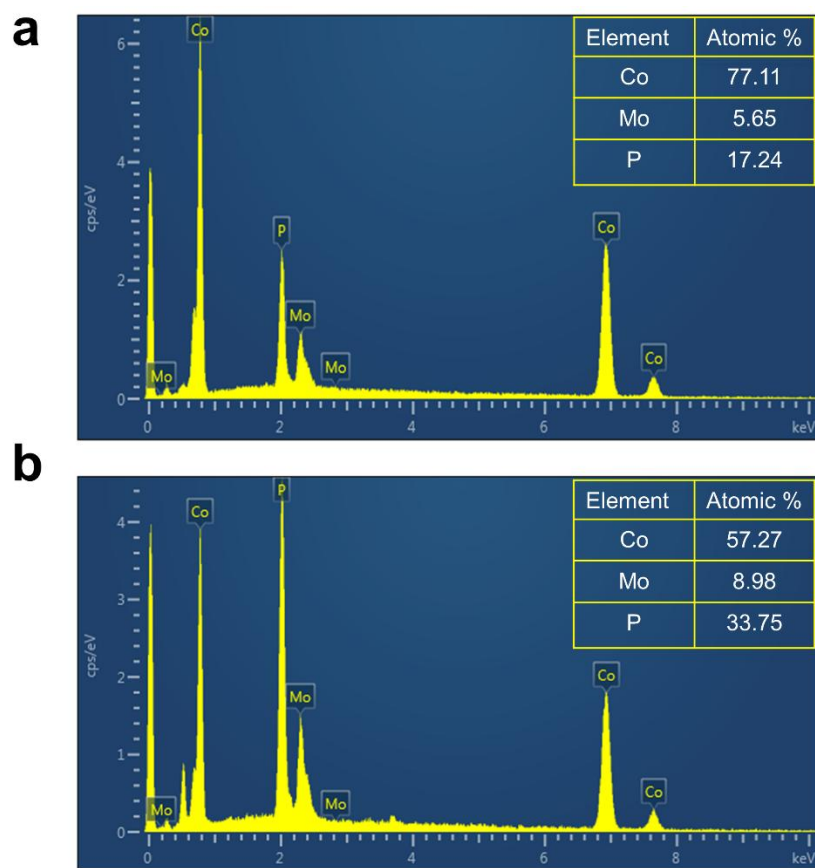


Figure S3. EDS spectra of $\text{Co}_{75}\text{Mo}_5\text{P}_{20}$ precursor alloy and np-Mo- Co_2P .

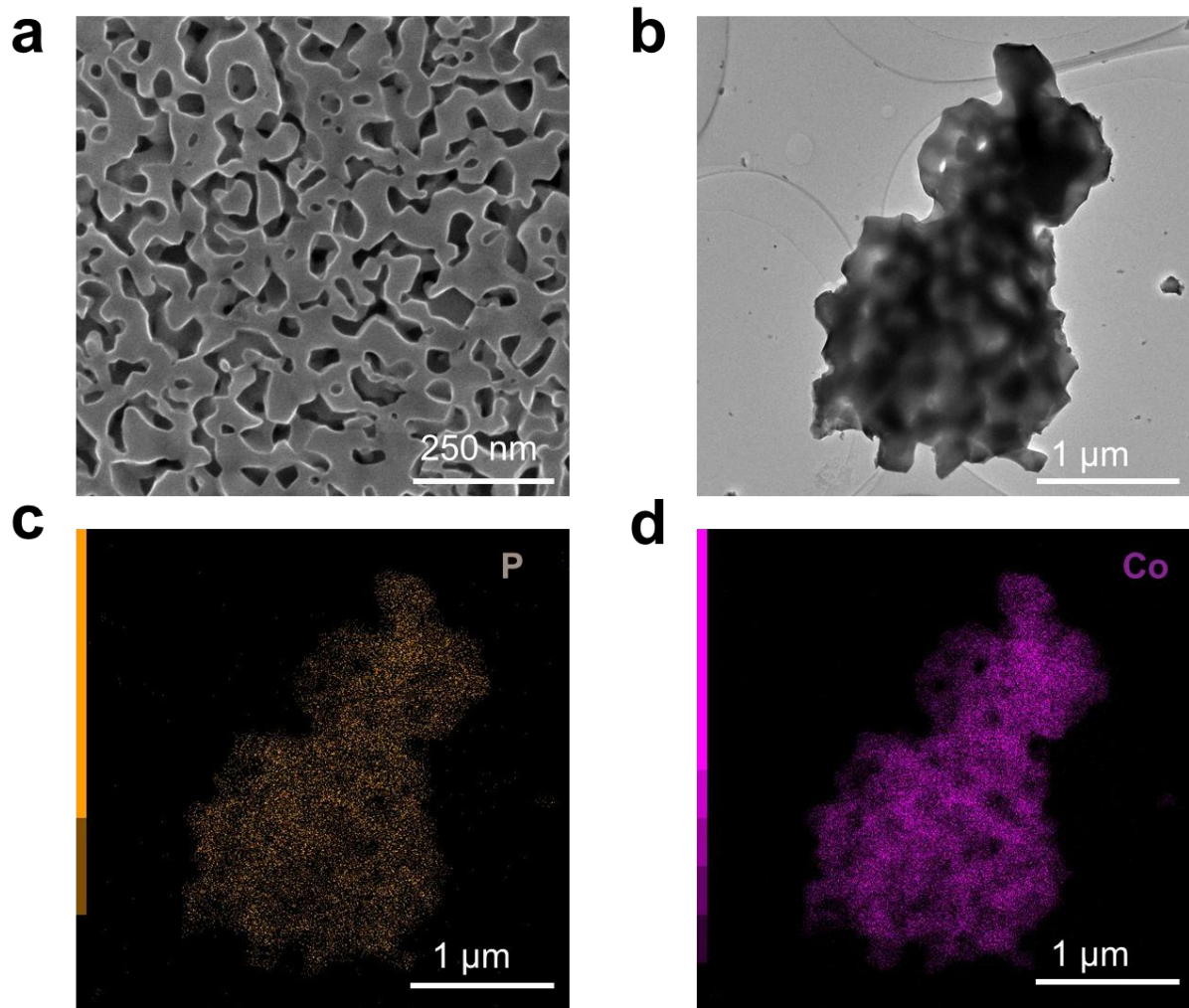


Figure S4. SEM, HADDF-STEM and EDS mapping images of np-Co₂P.

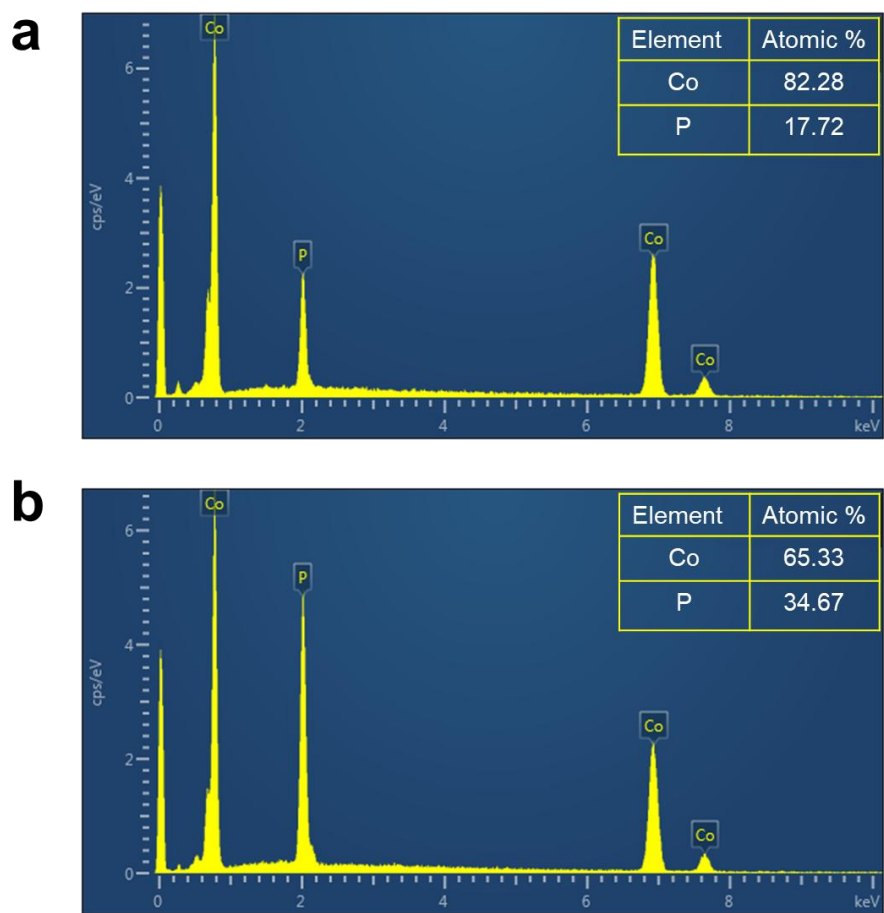


Figure S5. EDS spectra of (a) $\text{Co}_{80}\text{P}_{20}$ precursor alloy and (b) np- Co_2P .

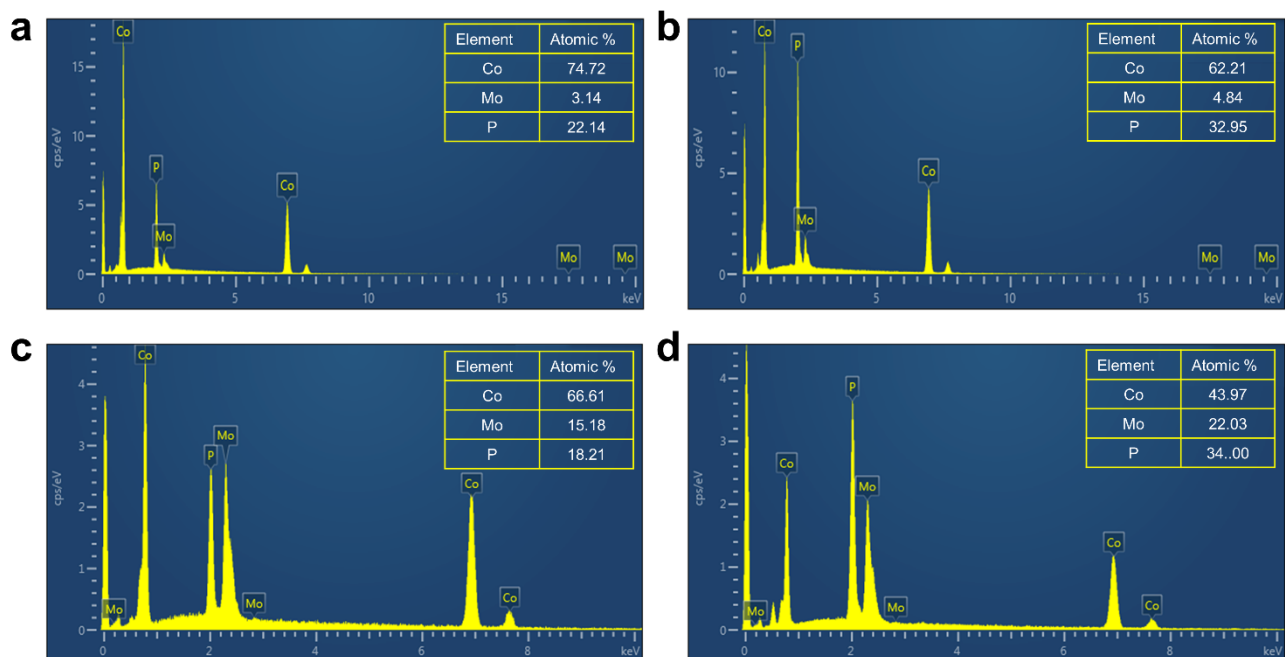


Figure S6. EDS spectra of (a) $\text{Co}_{77}\text{Mo}_3\text{P}_{20}$ and (c) $\text{Co}_{65}\text{Mo}_{15}\text{P}_{20}$ precursor alloy, and (b) np-Mo-Co₂P-1 and (d) Mo-Co₂P-3 catalysts.

*np-Mo-Co₂P-1 and np-Mo-Co₂P-3 correspond to lower and higher Mo contents, respectively, compared to np-Mo-Co₂P-2 (np-Mo-Co₂P), which serves as the primary sample discussed in this study.

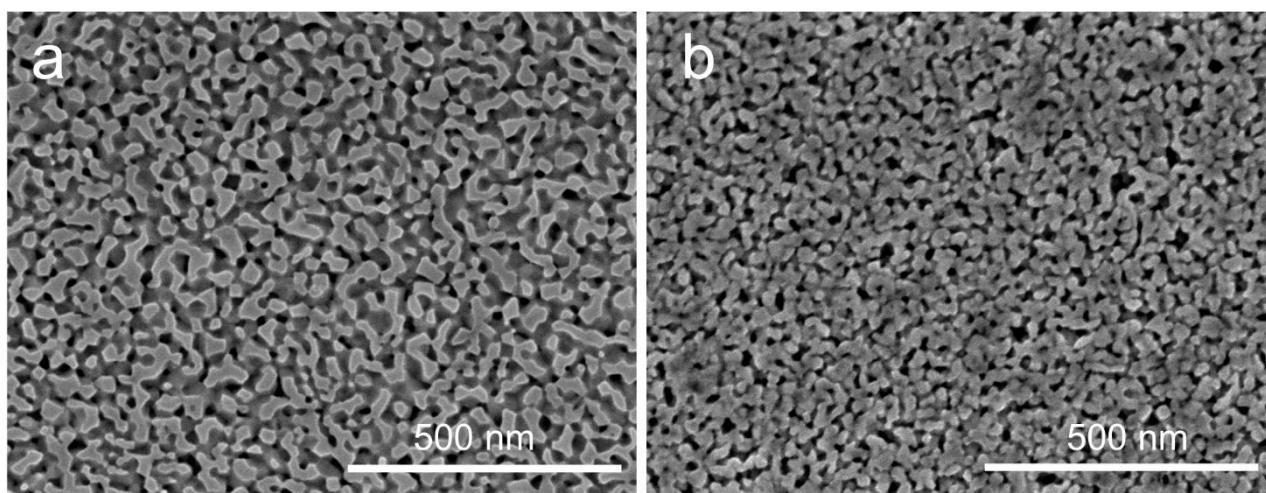


Figure S7. SEM images of np-Mo-Co₂P-1 and (d) Mo-Co₂P-3 catalysts.

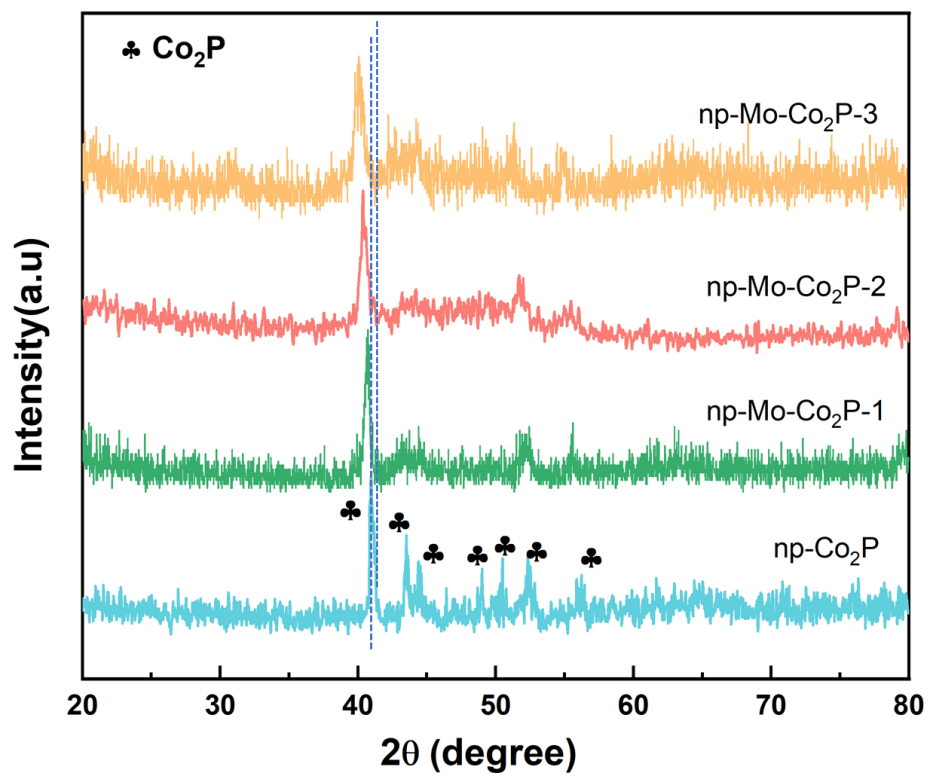


Figure S8. XRD patterns of np-Co₂P and (d) np-Mo-Co₂P-x (x=1, 2 or 3) catalysts.

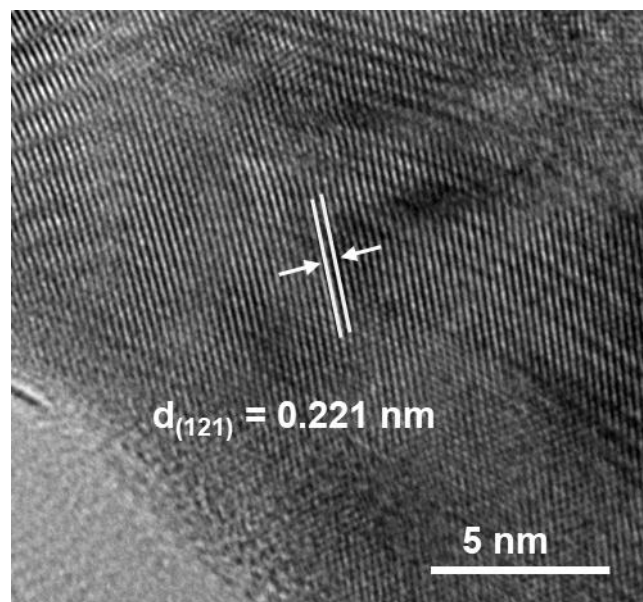


Figure S9. HRTEM image of np-Co₂P.

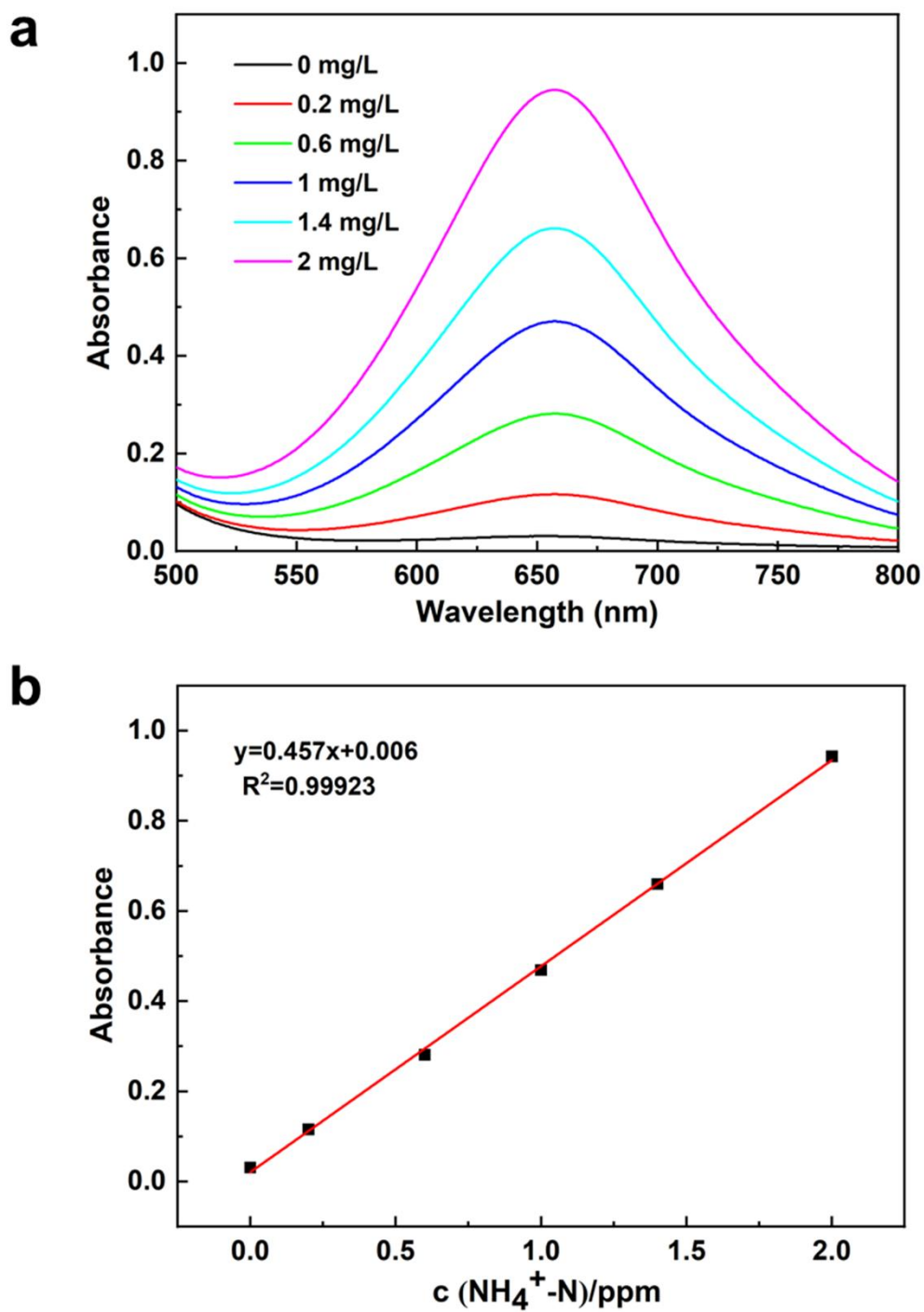


Figure S10. (a) UV-Vis absorption curves of the standard NH_3 solutions. (b) Calibration curves used for calculation of NH_3 concentration.

*The molar amount of NH_3 was calculated by converting the measured NH_4^+-N value to NH_3 .

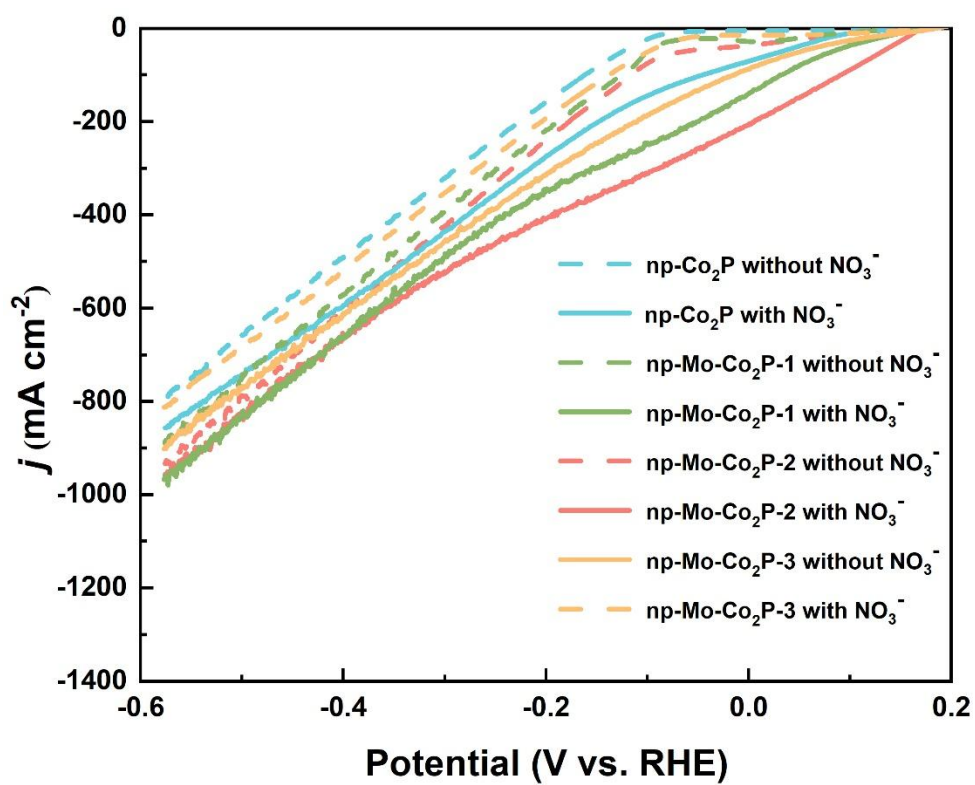


Figure S11. LSV curves of np-Co₂P and np-Mo-Co₂P-x (x=1, 2 or 3) catalysts in 1 M KOH with and without 0.1 M NO₃⁻.

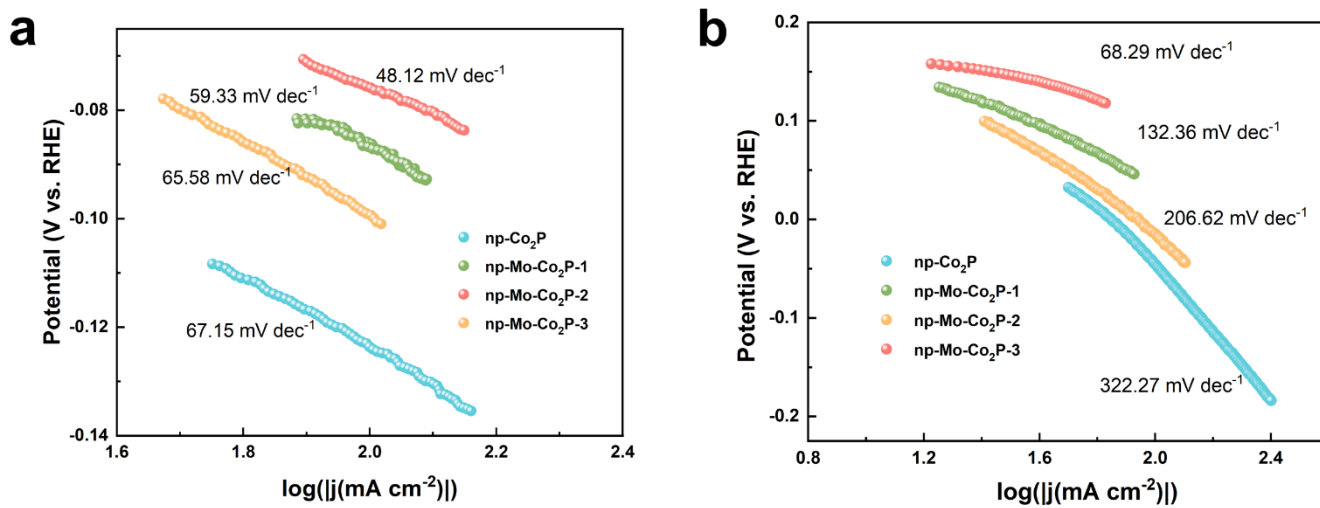


Figure S12. The Tafel plots of np-Co₂P and np-Mo-Co₂P-x (x=1, 2 or 3) catalysts in (a) 1 M KOH and (b) 1 M KOH + 0.1 M NO₃⁻.

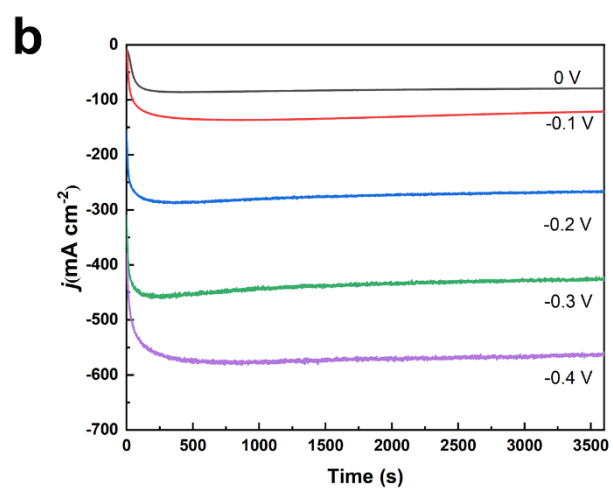
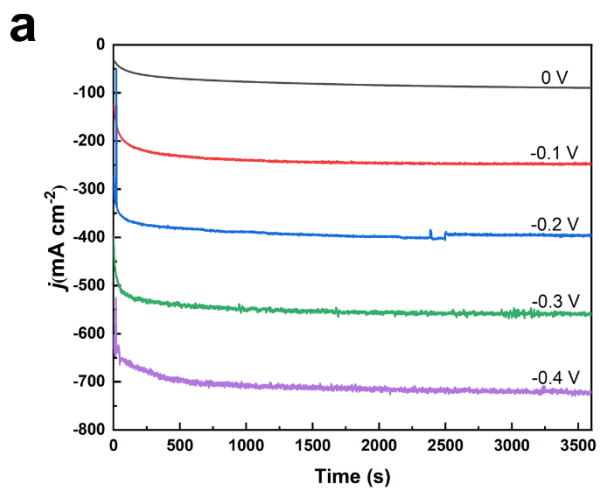


Figure S13. The i - t curves of (a) np-Mo-Co₂P and (b) np-Co₂P under different applied potential.

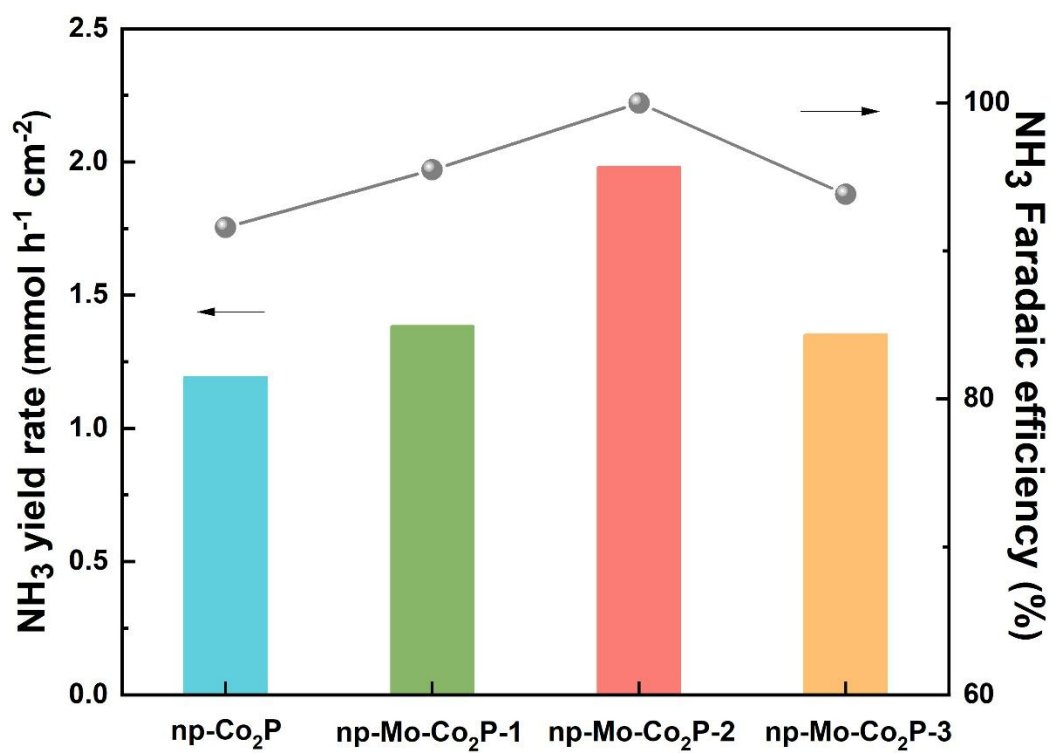


Figure S14. NH₃ yield rate and FE of np-Co₂P and np-Mo-Co₂P-x (x=1, 2 or 3) catalysts at -0.2 V vs.

RHE.

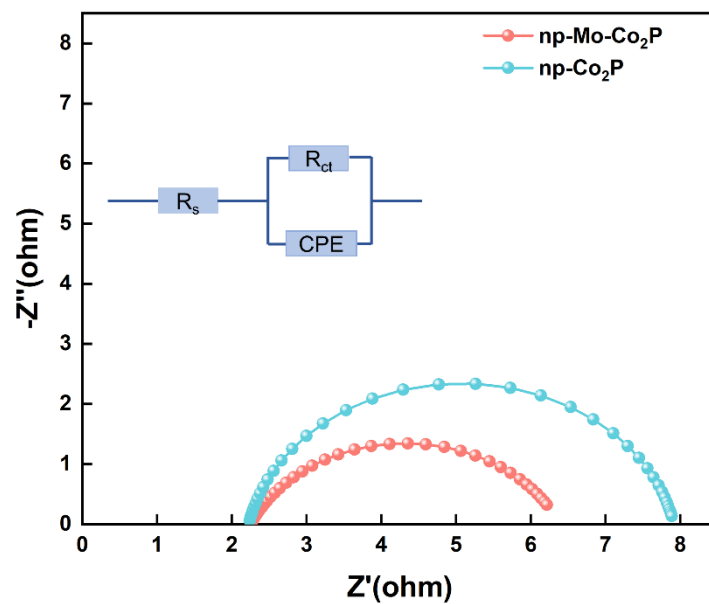


Figure S15. Nyquist plots of np-Mo-Co₂P and np-Co₂P catalysts in 1 M KOH and 0.1 M NO₃⁻.

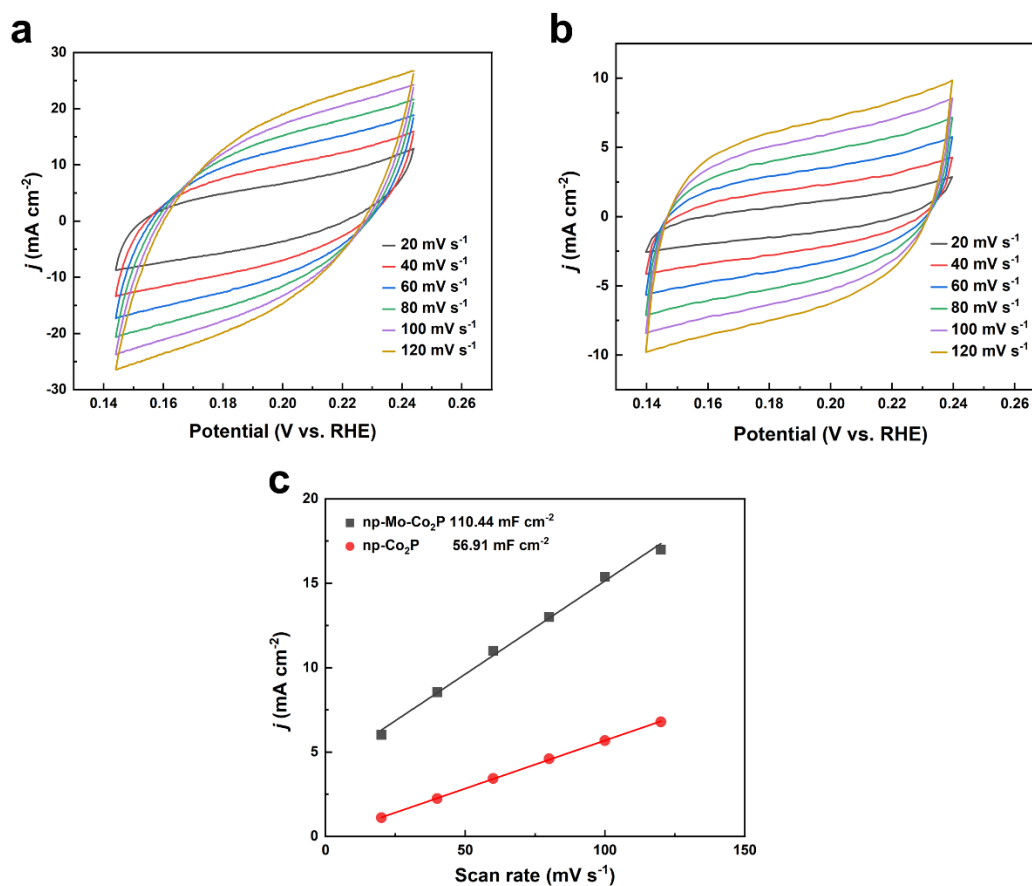


Figure S16. CV curves of (a) np-Mo-Co₂P and (b) np-Co₂P with different scan rates from 20 to 120 mV s⁻¹. (c) Plots of the current densities against CV scan rates for np-Mo-Co₂P and np-Co₂P, and the slope of the linear fit was the C_{dl} . The specific capacitance for a flat surface is assumed to be $40 \mu\text{F cm}^{-2}$. The

ECSA of catalysts was calculated as the following equation:

$$Catalyst_{ECSA} = \frac{C_{dl}}{40 \mu\text{F cm}^{-2} \text{ per cm}^2_{ECSA}}$$

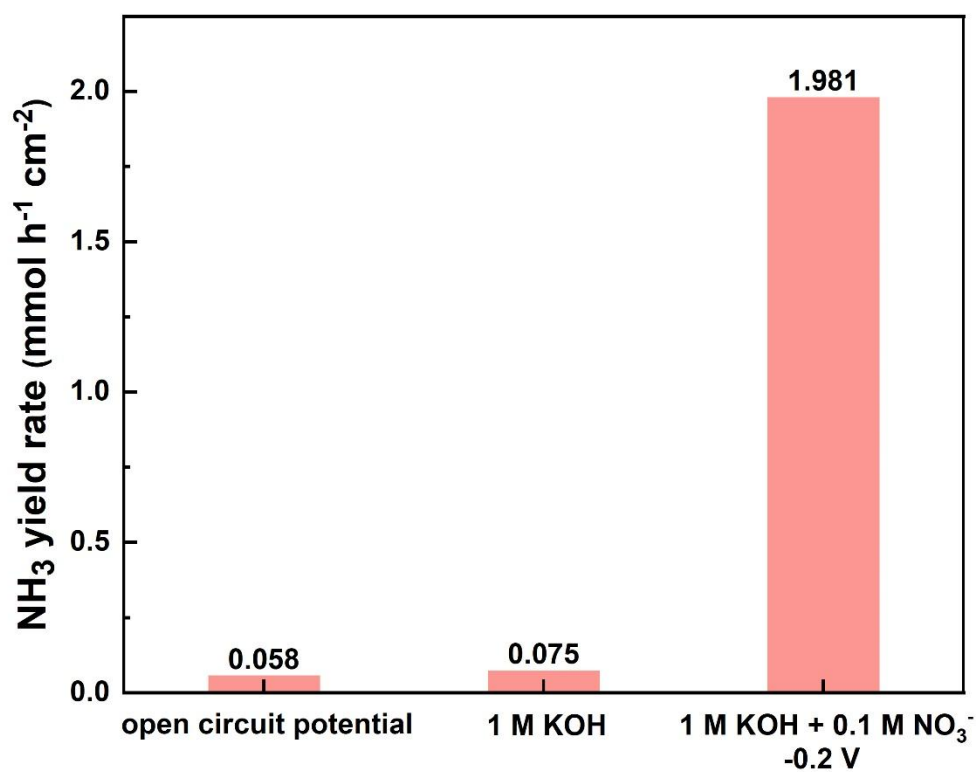


Figure S17. The NH₃ yield rate in 1 M KOH with 0.1 M NO₃⁻ at open circuit potential (OCP) and in 1 M KOH without 0.1 M NO₃⁻ at -0.2 V

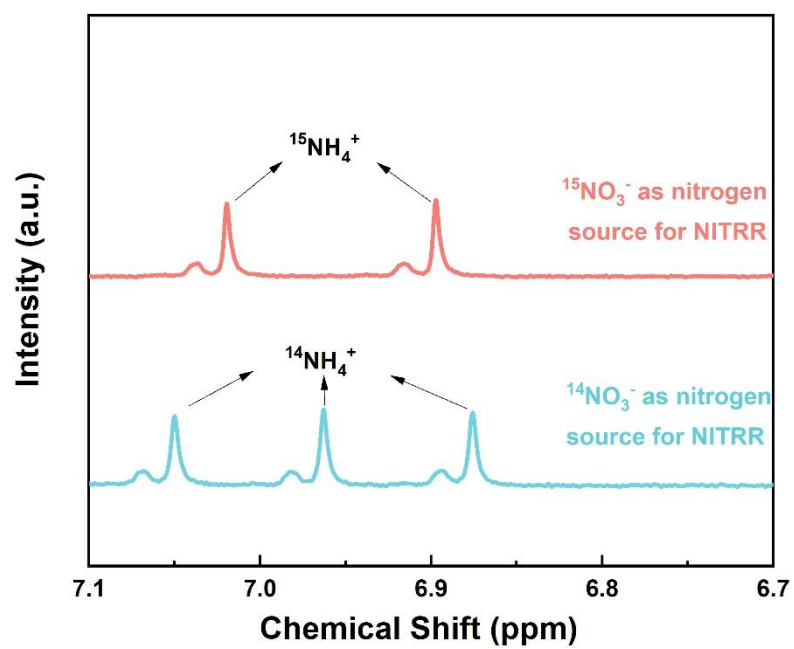


Figure S18. ^1H NMR spectra of the electrolyte after NITRR using $^{15}\text{NO}_3^-$ and $^{14}\text{NO}_3^-$ as the nitrogen source.

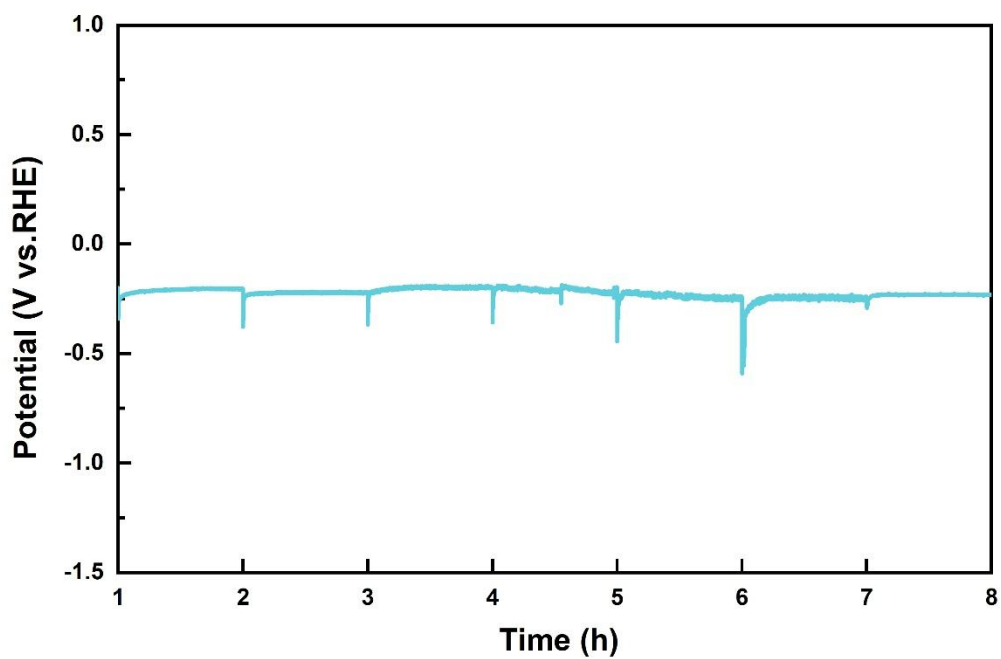


Figure S19. V-t curves of np-Mo-Co₂P catalyst at -400 mA cm⁻² for the stability test

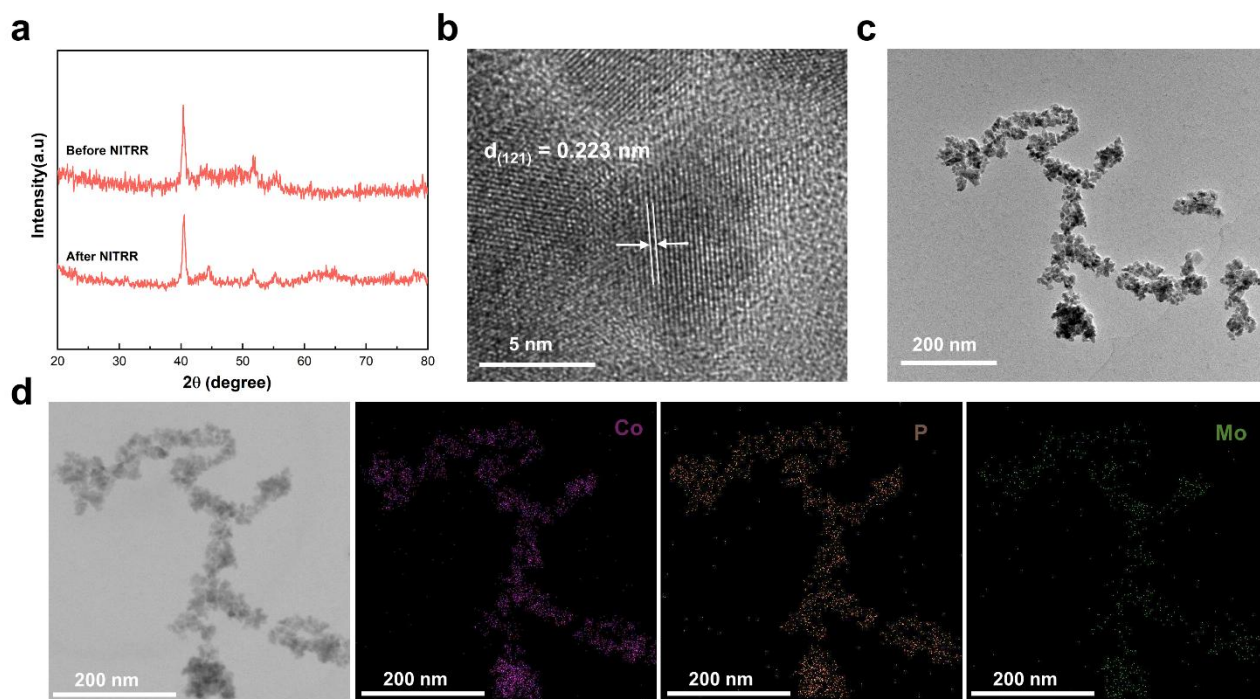


Figure S20. (a) XRD spectra of np-Mo-Co₂P before and after stability test. (b) HRTEM, (c) TEM, (d) HADDF-STEM and EDS mapping images of np-Mo-Co₂P after stability test.

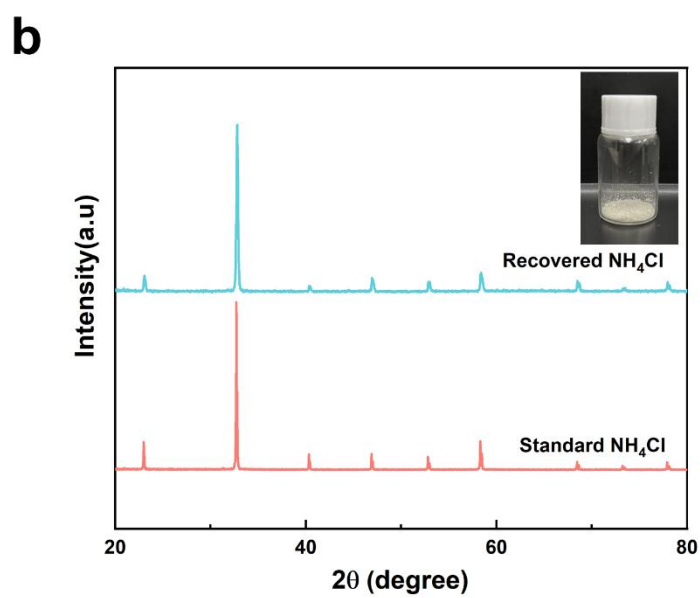
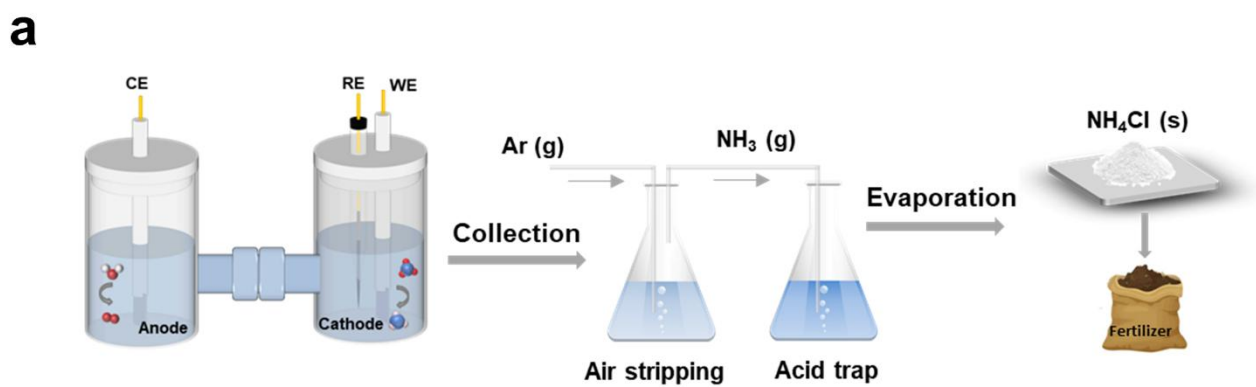


Figure S21. (a) Flow diagram for the recovery of NH₄Cl. (b) XRD patterns of the recovered and standard NH₄Cl. Inset is the optical image of recovered NH₄Cl.

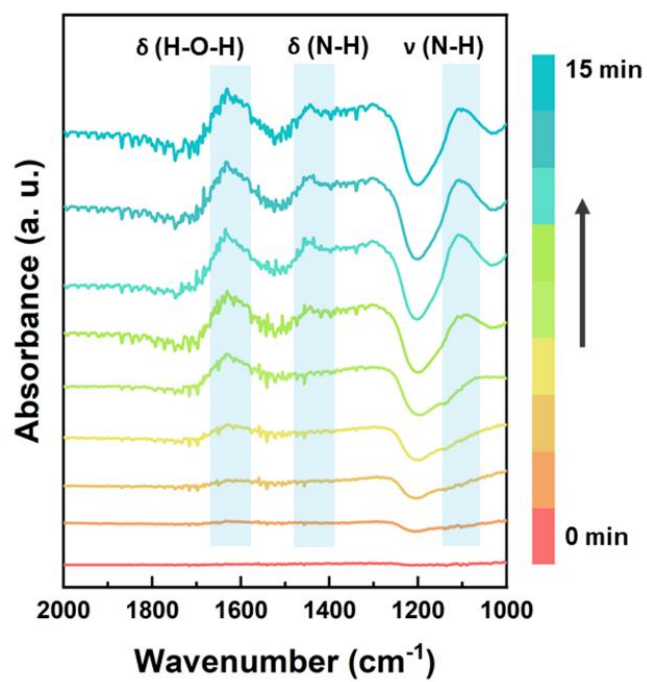


Figure S22. In-situ FTIR spectra of the intermediates on the np-Mo-Co₂P catalyst with time.

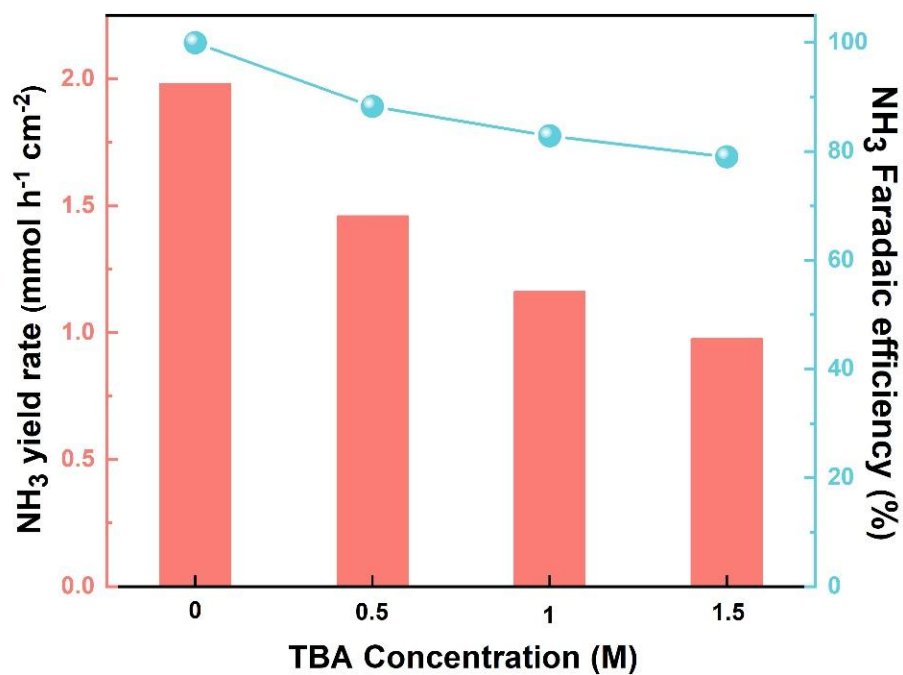


Figure S23. NH₃ yield rate and FE of np-Mo-Co₂P catalyst with the addition of various TBA concentration in 1 M KOH with 0.1 M NO₃⁻ electrolyte.

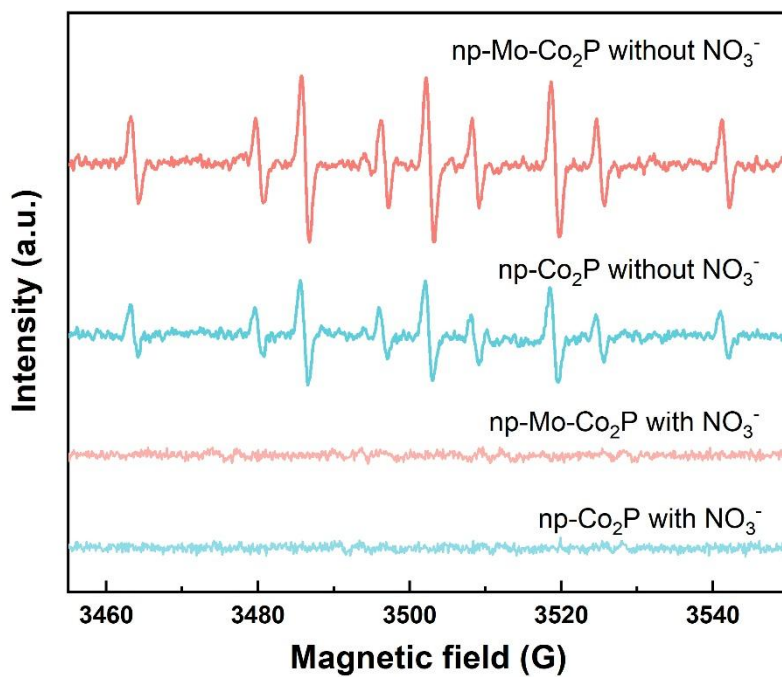


Figure S24. DMPO spin-trapping EPR spectra of np-Mo-Co₂P and np-Co₂P catalysts in different electrolytes.

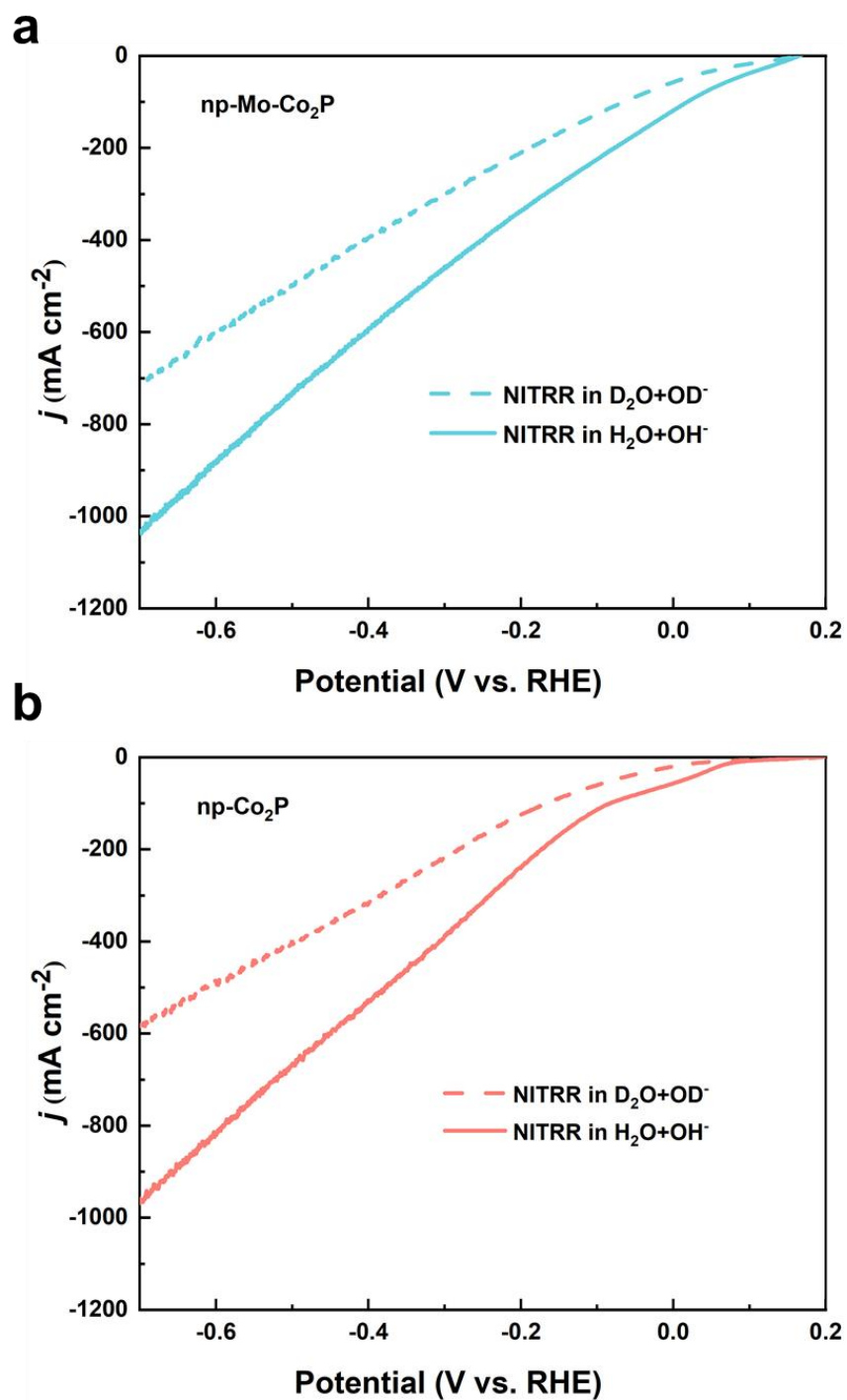
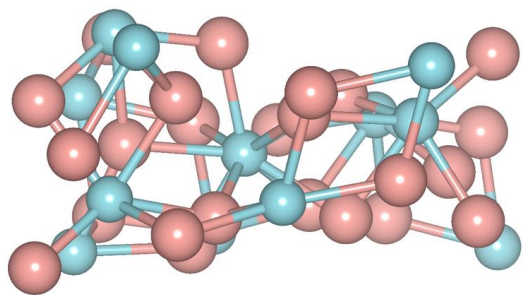


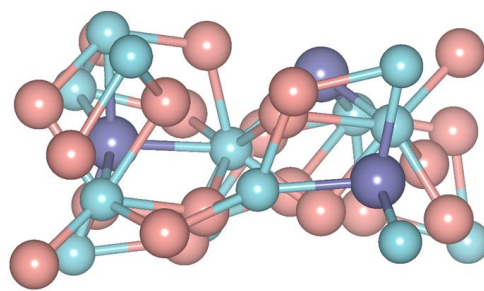
Figure S25. The LSV curves of (a) np-Mo-Co₂P and (b) np-Co₂P catalysts were recorded in electrolytes of 1 M KOH with 0.1 M NO₃⁻ in H₂O solvent, and 1 M KOD with 0.1 M NO₃⁻ in D₂O solvent.

a



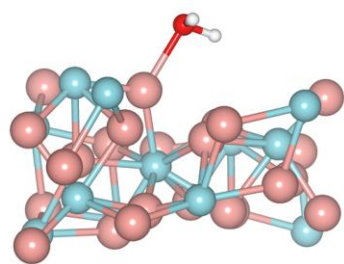
np-Co₂P

b

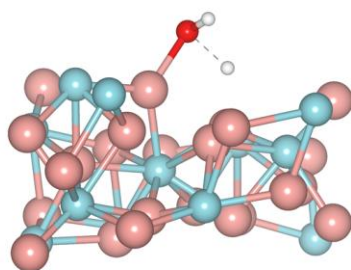


np-Mo-Co₂P

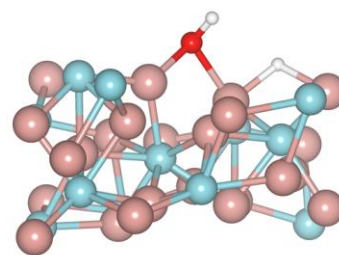
Figure S26. Stable configurations of np-Mo-Co₂P and np-Co₂P.



H₂O*



TS



*H+*OH

Figure S27. Stable configures of intermediates of H₂O dissociation on np-Co₂P.

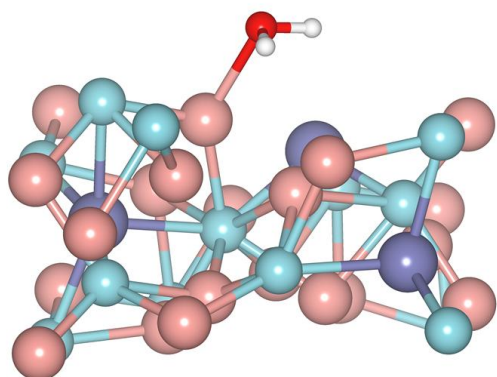
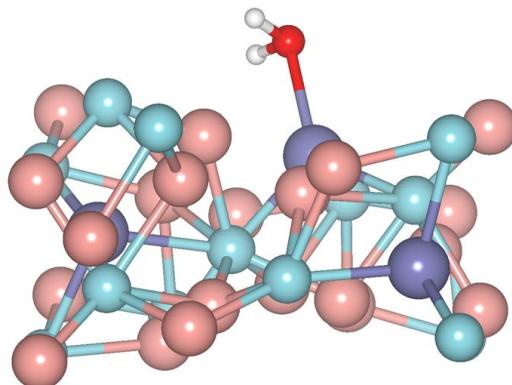
a**b**

Figure S28. Stable configurations of H₂O* on (a) Co site and (b) Mo site of np-Mo-Co₂P.

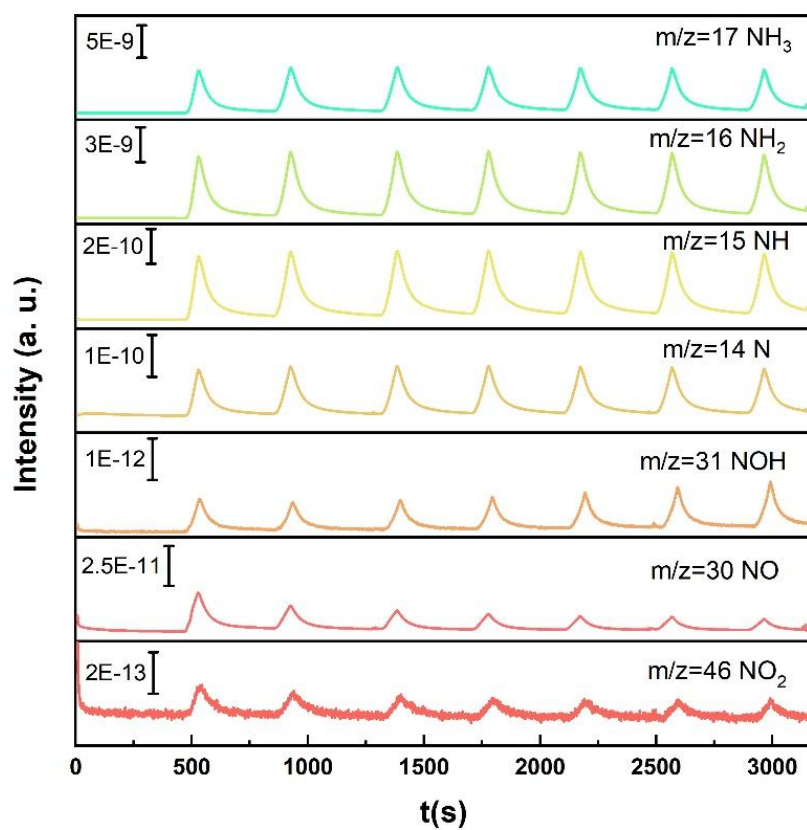


Figure S29. Electrochemical in-situ DEMS measurements of NITRR over np-Mo-Co₂P catalyst.

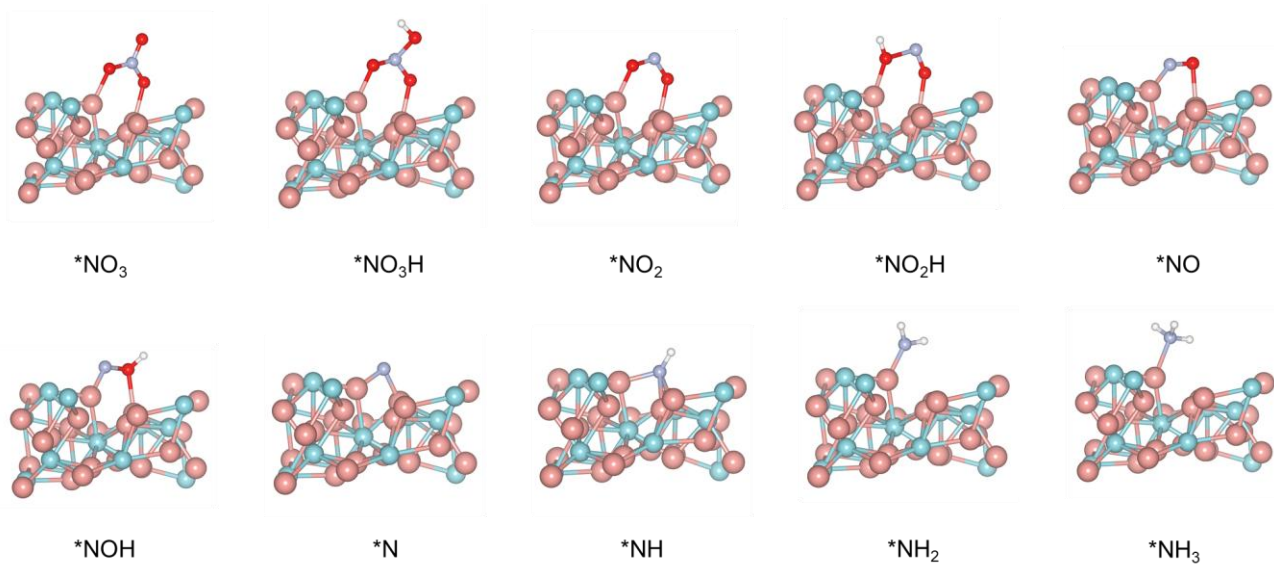


Figure S30. Stable configurations of intermediates on np-Co₂P during NITRR process.

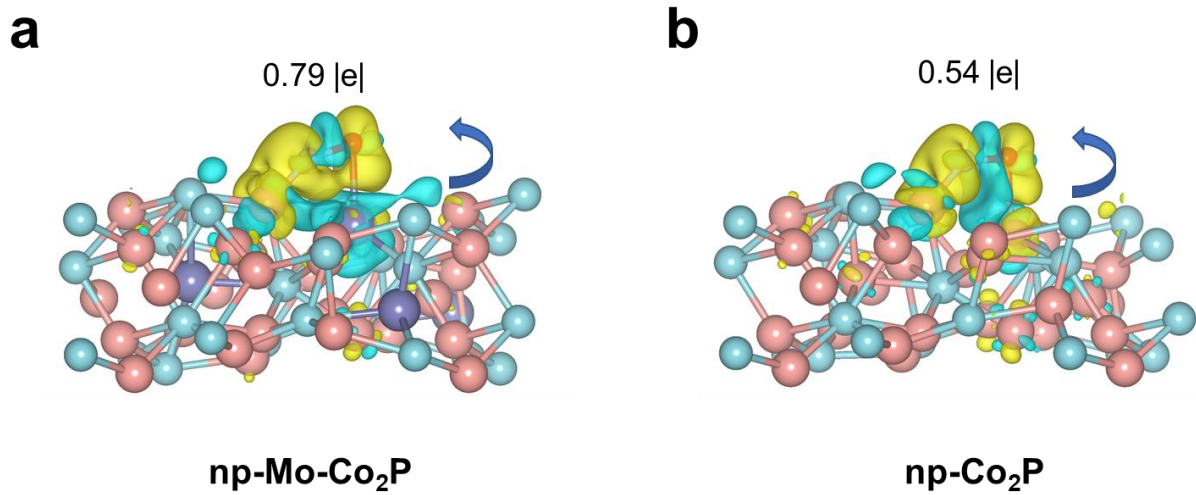


Figure S31. The charge density difference of adsorbed *NO on np-Mo-Co₂P.

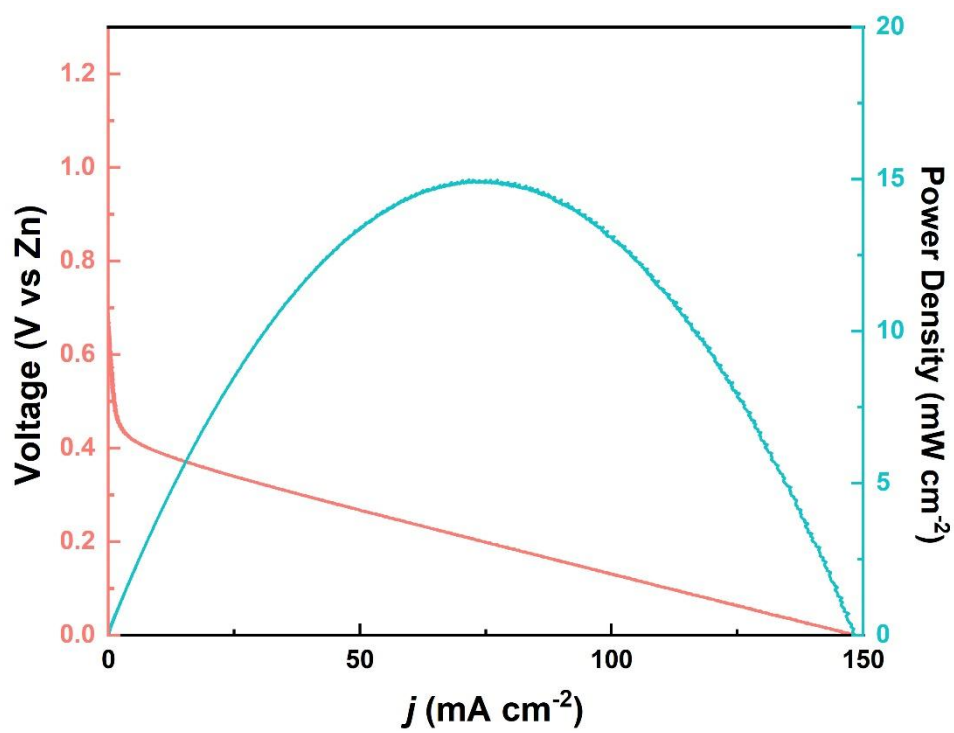


Figure S32. Discharging polarization curves and corresponding power densities of the np-Co₂P based Zn-NO₃⁻ battery.

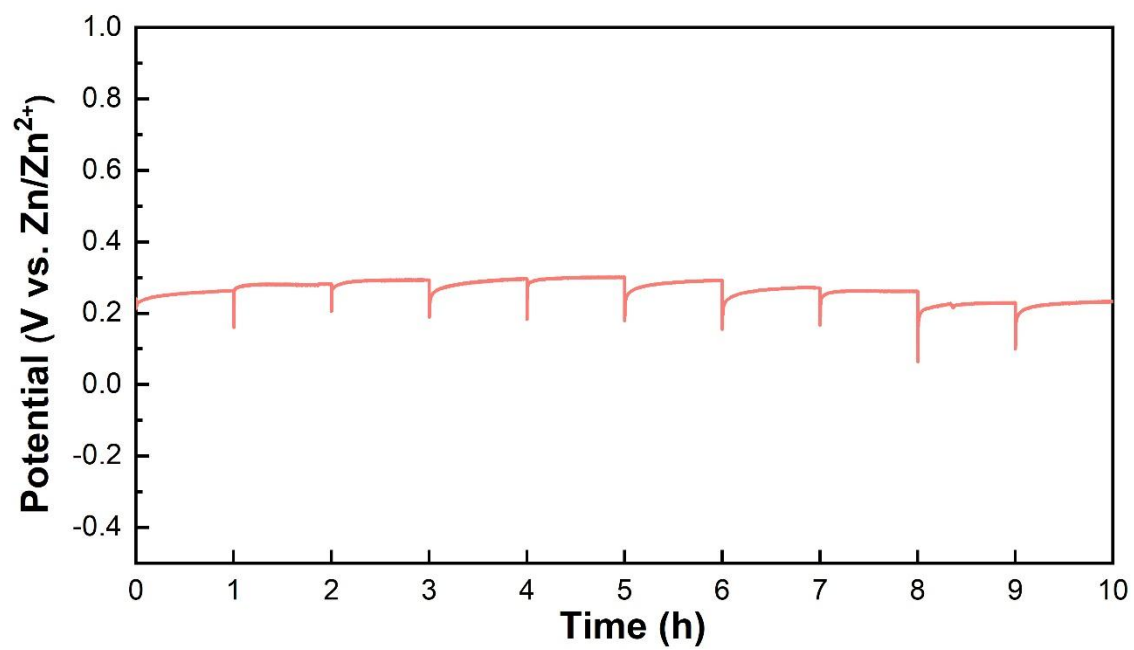


Figure S33. Discharged curves of the np-Mo-Co₂P based Zn-NO₃⁻ battery at 100 mA cm⁻² in stability test.

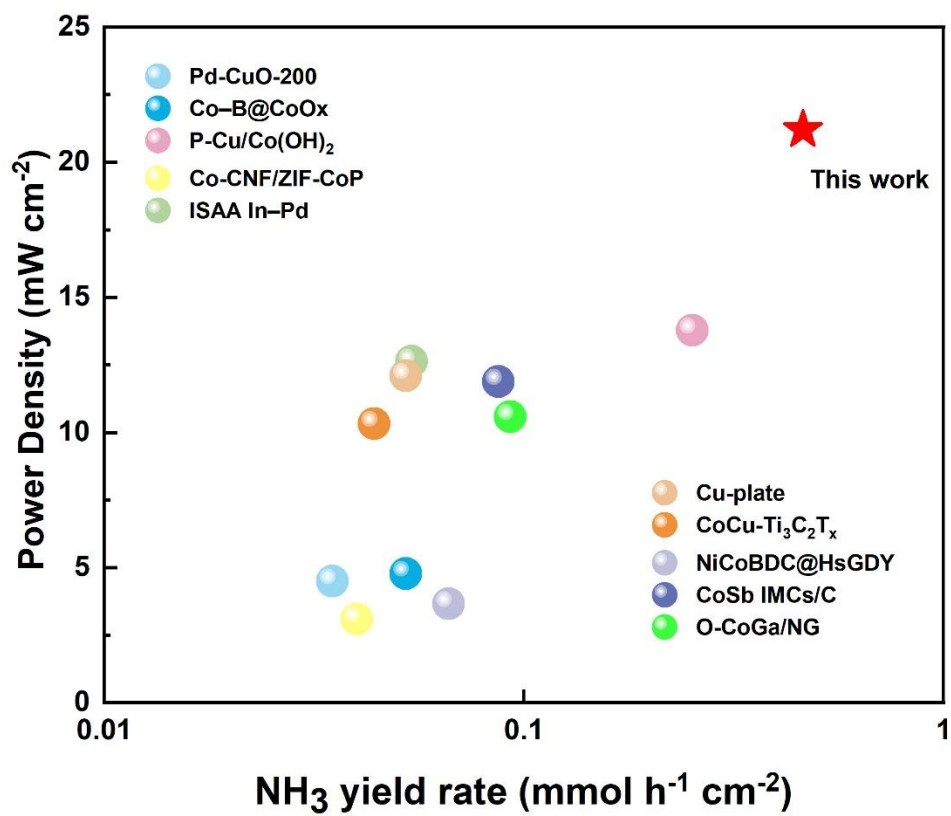


Figure S34. Comparison of the Zn-NO₃⁻ battery performance with the reported catalysts.

Table S1. Co, Mo and P content of np-Mo-Co₂P catalyst

Sample	Co (at.%)	Mo (at.%)	P (at.%)
np-Mo-Co ₂ P	57.86	8.91	33.23

Table S2. Comparison of NITRR performances of np-Mo-Co₂P with other reported catalyst.

Catalysts	Electrolyte	Potential (V vs. RHE)	NH ₃ yield rate (mmol h ⁻¹ cm ⁻²)	FE (%)	EE (%)	Ref.
np-Mo-Co₂P	1M KOH+ 0.1 M NO ₃ ⁻	-0.1	1.17 ± 0.19	100 ± 2.06	40.6	This work
		-0.2	1.98 ± 0.08	99.98± 0.93	37.75	
Pd-CuO-200	1 M KOH + 0.1 M NO ₃ ⁻	-0.5	0.924	90	28.09	4
CoCu-Ti ₃ C ₂ T _X	0.1 M K ₂ SO ₄ + 0.1 M NO ₃ ⁻	-0.7	0.48	93.6	26.19	5
NiCoBDC@H sGDY	1M KOH+ 0.1 M NO ₃ ⁻	-0.34	0.559	99.1	34.09	6
Ag/Co ₃ O ₄ /CoOOH	1M KOH+ 0.1 M NO ₃ ⁻	-0.25	0.254	94.3	34.41	7
Fe/Cu-NG	1 M KOH + 0.1 M NO ₃ ⁻	-0.3/-0.5	1.08 at -0.5	92.51 at -0.3	32.65	8
<i>meso-i</i> - AuCu ₃ @ <i>ultra</i> - Au	1 M KOH + 0.1 M NO ₃ ⁻	-0.55	0.622	96.24	29.20	9
FeB ₂	1M KOH+ 0.1 M NO ₃ ⁻	-0.6	1.5	96.8	28.56	10
np-CuCo	1 M KOH + 0.1 M NO ₃ ⁻	-0.23	0.837	91.5	33.84	11
Cu/Cu ₂ O NWAs	0.5 M Na ₂ SO ₄ + 200 ppm NO ₃ ⁻ - N	-0.85	0.24	95.8	29.06	12
CoSb IMCs	0.1 M KOH + 500 ppm NO ₃ ⁻ - N	-0.55/-0.65	0.29 at -0.65 V	96.3 at -0.55	30.34	13
PR-CuNC	0.1 M KOH + 0.1 M NO ₃ ⁻	-0.5	0.22	94.61	29.53	14
Ag-Co ₃ O ₄	0.1 M KOH + 0.1 M NO ₃ ⁻	-0.32	0.052	88	30.66	15

Table S3. Impedance studies of np-Mo-Co₂P and np-Co₂P catalyst

Sample	R_s (Ω)	R_{ct} (Ω)
np-Mo-Co ₂ P	2.251	4.143
np-Co ₂ P	2.228	5.689

Table S4. Metal (Co and Mo) content of the electrolyte after stability test

Sample	Co (ppm)	Mo (ppm)
After stability test	0.000	0.003

Table S5. Adsorption energy of H₂O at different sites of np-Mo-Co₂P.

Sample	E_{ads}(eV)
Mo site	-1.19
Co site	-0.78

Table S6. Number of electrons gained and lost by Mo, Co and P atoms in np-Mo-Co₂P. Negative value represents electron loss, while positive value represents electro gain.

Sample	Atom	Valence electrons	Electric charge	Electron number
np-Mo-Co ₂ P	Co1	9	8.9203	0.0797
	Co2	9	8.94607	0.05393
	Co3	9	9.02797	-0.02797
	Co4	9	8.88295	0.11705
	Co5	9	8.70687	0.29313
	Co6	9	8.89452	0.10548
	Co7	9	8.94449	0.05551
	Co8	9	8.91675	0.08325
	Co9	9	8.85022	0.14978
	Co10	9	8.794	0.206
	Co11	9	8.90925	0.09075
	Co12	9	8.84782	0.15218
	Co13	9	8.90637	0.09363
	Co14	9	8.85227	0.14773
	Co15	9	8.78699	0.21301
	Co16	9	8.8041	0.1959
	Co17	9	8.93743	0.06257
	Co18	9	9.00422	0.00422
	Co19	9	8.89208	0.10792
	Co20	9	8.84032	0.15968
	Co21	9	8.79831	0.20169
	Mo1	14	13.34641	0.65359
	Mo2	14	13.06239	0.93761
	Mo3	14	13.18522	0.81478
P1	5	5.39089	-0.39089	
P2	5	5.3993	-0.3993	
P3	5	5.48415	-0.48415	
P4	5	5.37073	-0.37073	
P5	5	5.51645	-0.51645	
P6	5	5.21675	-0.21675	
P7	5	5.36374	-0.36374	
P8	5	5.54537	-0.54537	
P9	5	5.3596	-0.3596	
P10	5	5.45122	-0.45122	
P11	5	5.45913	-0.45913	
P12	5	5.38537	-0.38537	

Table S7. Number of electrons gained and lost by Co and P atoms in np-Co₂P. Negative value represents electron loss, while positive value represents electro gain.

Sample	Atom	Valence electrons	Electric charge	Electron number
np-Co ₂ P	Co1	9	8.93726	-0.06274
	Co2	9	8.9142	-0.0858
	Co3	9	8.86978	-0.13022
	Co4	9	8.77824	-0.22176
	Co5	9	8.68135	-0.31865
	Co6	9	8.85428	-0.14572
	Co7	9	8.8208	-0.1792
	Co8	9	8.88971	-0.11029
	Co9	9	8.85697	-0.14303
	Co10	9	8.84364	-0.15636
	Co11	9	8.71698	-0.28302
	Co12	9	8.75654	-0.24346
	Co13	9	8.88828	-0.11172
	Co14	9	8.84058	-0.15942
	Co15	9	8.88966	-0.11034
	Co16	9	8.85672	-0.14328
	Co17	9	8.76696	-0.23304
	Co18	9	8.81442	-0.18558
	Co19	9	8.93757	-0.06243
	Co20	9	8.92916	-0.07084
	Co21	9	8.82833	-0.17167
	Co22	9	8.82039	-0.17961
	Co23	9	8.77457	-0.22543
	Co24	9	8.79113	-0.20887
P1	5	5.29651	0.29651	
P2	5	5.32643	0.32643	
P3	5	5.31685	0.31685	
P4	5	5.39039	0.39039	
P5	5	5.36052	0.36052	
P6	5	5.19415	0.19415	
P7	5	5.27366	0.27366	
P8	5	5.43278	0.43278	
P9	5	5.27398	0.27398	
P10	5	5.39175	0.39175	
P11	5	5.36731	0.36731	
P12	5	5.31816	0.31816	

Table S8. Comparison of Zn-NO₃⁻ battery performances of np-Mo-Co₂P with other reported catalyst.

Catalysts	Electrolyte in cathode	Electrolyte in Anode	Power density (mW cm ⁻²)	NH ₃ yield rate (mmol h ⁻¹ cm ⁻²)	Ref.
Pd-CuO-200	1 M KOH+ 0.1 M NO ₃ ⁻	6 M KOH	4.5	0.035	4
Co-B@CoOx	0.5 M Na ₂ SO ₄ + 100 ppm NO ₃ ⁻ - N	1 M KOH	4.78	0.052	16
P-Cu/Co(OH) ₂	1 M KOH+ 0.1 M NO ₃ ⁻	3 M KOH	13.78	0.252	17
Co-CNF/ZIF-CoP	1 M KOH+ 0.1 M NO ₃ ⁻	3 M KOH	3.1	0.040	18
ISAA In-Pd	0.5 M Na ₂ SO ₄ + 100 ppm NO ₃ ⁻ - N	1 M KOH	12.64	0.054	19
Cu-plate	1 M KOH+ 0.5 M NO ₃ ⁻	1 M KOH	12.09	0.052	20
CoCu-Ti ₃ C ₂ Tx	0.5 M K ₂ SO ₄ + 0.1 M NO ₃ ⁻	1 M KOH	10.33	0.044	5
NiCoBDC@HsGDY	1 M KOH+ 0.1 M NO ₃ ⁻	6 M KOH	3.66	0.066	6
CoSb IMCs/C	1 M KOH+ 0.1 M NO ₃ ⁻	1 M KOH	11.88	0.087	13
O-CoGa/NG	1 M KOH+ 0.1 M NO ₃ ⁻	1 M KOH	10.58	0.093	21
np-Mo-Co₂P	1 M KOH+ 0.1 M NO₃⁻	6 M KOH	21.30	0.463	This work

References

- 1 G. Kresse, J. Furthmüller, *Phys. Rev. B*, 1996, **54**, 11169.
- 2 J. P. Perdew, K. Burke, M. Ernzerhof, *Phys. Rev. Lett.*, 1996, **77**, 3865.
- 3 P. E. Blöchl, *Phys. Rev. B*, 1994, **50**, 17953.
- 4 Y. Liu, Z. Zhuang, Y. Liu, N. Liu, Y. Li, Y. Cheng, J. Yu, R. Yu, D. Wang, H. Li, *Angew. Chem. Int. Ed.*, 2024, **63**, e202411396.
- 5 Z. Cui, P. Zhao, H. Wang, C. Li, W. Peng, J. Liu, *Adv. Funct. Mater.*, 2024, **34**, 2410941.
- 6 J. Ma, Y. Zhang, B. Wang, Z. Jiang, Q. Zhang, S. Zhuo, *ACS Nano*, 2023, **17**, 6687.
- 7 S. Wu, Y. Jiang, W. Luo, P. Xu, L. Huang, Y. Du, H. Wang, X. Zhou, Y. Ge, J. Qian, H. Nie, Z. Yang, *Adv. Sci.*, 2023, **10**, 2303789.
- 8 S. Zhang, J. Wu, M. Zheng, X. Jin, Z. Shen, Z. Li, Y. Wang, Q. Wang, X. Wang, H. Wei, J. Zhang, P. Wang, S. Zhang, L. Yu, L. Dong, Q. Zhu, H. Zhang, J. Lu, *Nat. Commun.*, 2023, **14**, 3634.
- 9 Y. Xiao, X. Tan, B. Du, Y. Guo, W. He, H. Cui, C. Wang, *Angew. Chem. Int. Ed.*, 2024, **63**, e202408758.
- 10 G. Zhang, X. Li, K. Chen, Y. Guo, D. Ma, K. Chu, *Angew. Chem. Int. Ed.*, 2023, **62**, e202300054.
- 11 X. Zhou, W. Xu, Y. Liang, H. Jiang, Z. Li, S. Wu, Z. Gao, Z. Cui, S. Zhu, *ACS Catal.*, 2024, **14**, 12251.
- 12 Y. Wang, W. Zhou, R. Jia, Y. Yu, B. Zhang, *Angew. Chem. Int. Ed.*, 2020, **59**, 5350.
- 13 C. Ma, H. Zhang, J. Xia, X. Zhu, K. Qu, F. Feng, S. Han, C. He, X. Ma, G. Lin, W. Cao, X. Meng, L. Zhu, Y. Yu, A.-L. Wang, Q. Lu, *J. Am. Chem. Soc.*, 2024, **146**, 20069.
- 14 Y. Liu, W. Qiu, P. Wang, R. Li, K. Liu, K. M. Omer, Z. Jin, P. Li, *Appl. Catal., B*, 2024, **340**, 123228.
- 15 M. Zhang, Z. Ma, S. Zhou, C. Han, V. Kundi, P. V. Kumar, L. Thomsen, B. Johannessen, L. Peng, Y. Shan, C. Tsounis, Y. Yang, J. Pan, R. Amal, *ACS Catal.*, 2024, **14**, 11231.
- 16 X. Zhu, C. Ma, Y.-C. Wang, K. Qu, L. Song, J. Wang, Y. Gong, X. Liu, J. Zhang, Q. Lu, A.-L. Wang, *Energy Environ. Sci.*, 2024, **17**, 2908.
- 17 Q. Yan, R. Zhao, L. Yu, Z. Zhao, L. Liu, J. Xi, *Adv. Mater.*, 2024, **36**, 2408680.
- 18 R. Qi, Z. Wang, M. Zhong, C. Wang, F. Bai, X. Lu, *Small*, 2023, **20**, 2308311.
- 19 M. Xie, S. Tang, Z. Li, M. Wang, Z. Jin, P. Li, X. Zhan, H. Zhou, G. Yu, *J. Am. Chem. Soc.*, 2023, **145**, 13957.
- 20 L. Zhou, X. Chen, S. Zhu, K. You, Z. J. Wang, R. Fan, J. Li, Y. Yuan, X. Wang, J. Wang, Y. Chen, H. Jin, S. Wang, J. J. Lv, *Angew. Chem. Int. Ed.*, 2024, **63**, e202401924.
- 21 H. Zhang, C. Ma, Y. C. Wang, X. Zhu, K. Qu, X. Ma, C. He, S. Han, A. H. Liu, Q. Wang, W. Cao, W. Lin, J. Xia, L. Zhu, L. Gu, Q. Yun, A. L. Wang, Q. Lu, *Angew. Chem. Int. Ed.*, 2024, **63**, e202409515.